Agricultural and Forest Meteorology 221 (2016) 152–163

Contents lists available at ScienceDirect

Agricultural and Forest Meteorology

journal homepage: www.elsevier.com/locate/agrformet

Modeling short wave solar radiation flux in a trench water harvesting system

Nurit Agam*, Solomon Leake, Pedro R. Berliner

Blaustein Institutes for Desert Research, Ben-Gurion University of the Negev, Israel

ARTICLE INFO

Article history:
Received 11 December 2015
Received in revised form 11 February 2016
Accepted 15 February 2016

Keywords:
Shortwave radiation
Trench orientation
Rainwater harvesting
Radiation model

ABSTRACT

Micro-catchment water harvesting systems are systems by which runoff is collected from a contributing area, stored in an adjacent infiltration basin, and support tree growth during the dry season. Increase of the efficiency of such systems can be achieved by minimizing non-productive water losses, which mainly occur from the impounding area during the period during which free water is available and from the wet soil surface thereafter. Designing the infiltration basin as a trench can potentially meet this goal. The main driver for water loss through evaporation is the flux of short wave radiation that reaches the wetted surface. The first step in developing a comprehensive model to this effect, and the objective of the work reported herein is to model the short wave radiative fluxes for different trench geometries. The model computes the radiation reaching the floor of a trench at each point across the trench width accounting for the direct, diffuse, and reflected components. Model validation indicated that the model accurately depicts the diurnal course of radiation reaching the trench floor in both north-south and east-west orientated trenches in both summer and winter. Simulations for the Negev Desert revealed distinct differences in the diurnal course of mean solar radiation reaching the trench floor between north-south and east-west orientations. During the rainy season (November through March) radiation load was found to be greater in the north-south orientation. Thus, aiming to reduce evaporative losses from trench-like runoff harvesting systems in the Negev, east-west orientated trenches are advantageous.

1. At issue

Drylands occupy about 41% of Earth's land surface, and while being home to about one third of the human population, they retain only 8% of the world's renewable water resources (Millennium Ecosystem Assessment, 2005). For thousands of years man has tried to skillfully manage this vital but scarce resource by collecting runoff water and utilizing it for irrigation (e.g., Evenari et al., 1971; Droppelmann and Berliner, 2003). Water harvesting methods formerly developed for mere existence (Boers and Benasher, 1982) are nowadays receiving renewed attention.

Micro-catchment water harvesting systems, used in many dryland areas around the world (e.g., Critchley and Siegert, 1991) are systems by which runoff is collected from a contributing area, stored in an adjacent infiltration basin, and support tree growth during the dry season (Boers and Benasher, 1982). Micro-catchment systems were developed and implemented in Mediterranean climates in which the dry season can be very long. In order to ensure tree production, non-productive water losses have to be minimized. Water losses mainly occur from the impounding area during the period during which free water is available and from the wet soil surface thereafter. The surface of the wetted area thus plays a major role (Zhang et al., 2013). Traditionally, the infiltration basins of micro-catchment systems were shallow (Fig. 1a) and deepening them significantly reduced evaporation from the soil surface (Zhang et al., 2013). It is, however, not practical to dig deep pits for each tree and the use of trenches has been proposed (Fig. 1b). The depth of the trench directly affects costs and it is therefore of interest to estimate the relation between trench geometry and water loss. The main driver for evaporation is the flux of short wave radiation that reaches the wetted surface. The first step in developing a comprehensive model to this effect, and the objective of the work reported herein is to model the short wave radiative fluxes for different trench geometries (depth/width and orientation).

Solar radiation intensity at a given point is the sum of the direct beam radiation, solar radiation scattered during its passage through the atmosphere (diffuse radiation), and the radiation reflected downwards by the walls of the trench. The relative contribution, and thus the relative importance of each of the above mentioned

* Corresponding author.
E-mail address: agam@bgu.ac.il (N. Agam).

http://dx.doi.org/10.1016/j.agrformet.2016.02.014
0168-1923/

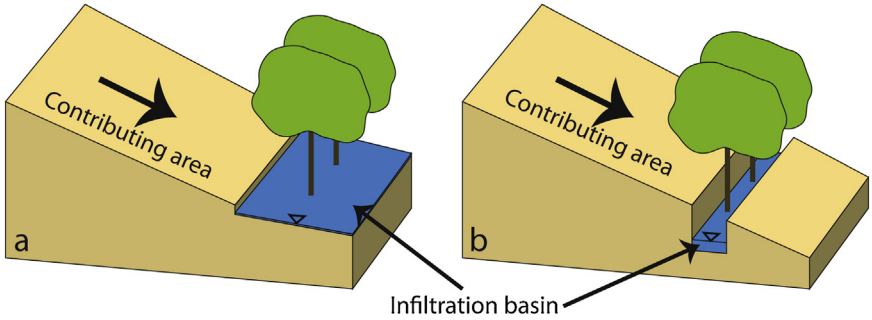

Fig. 1. Micro-catchment systems design. (a) Traditional design with larger and shallow infiltration basin; and (b) trench design with a deep infiltration basin.

components, varies depending on the geometry of the trench, the geographic location, the season and environmental parameters. In urban canyons, to which the system studied here resemble somewhat, reflected radiation may become a significant component (Erell and Williamson, 2006).

Models describing short wave radiation flux in urban canyons typically parametrize the optical properties of the canyon through the sky view factor (SVF) (SVF; e.g., Terjung and Orourke, 1980a,b; Erell and Williamson, 2006). The SVF defines the extent to which any point on a surface is open to the sky (Oke, 1988). Typically, the SVF is calculated for the center point of a symmetric canyon of infinite length based on the model developed by Oke (1981). This method has the advantage of ease of implementation. However, it does not allow the inclusion of irregular features such as tree canopy. The output of the model described hereafter is the shortwave radiation reaching each point across the trench width without the presence of plant canopies. Inclusion of canopy can be easily implemented and thus provides the flexibility necessary to model agricultural systems.

2. Model description

The model treats separately the three components of solar radiation reaching the bottom of a trench: the direct solar radiation, the diffuse radiation emanating from the portion of the sky hemisphere, and the downward reflected radiation from the trenches walls.

2.1. Direct solar radiation

The direct radiation can either reach the bottom of the trench, its intensity being equal to the direct radiation outside the trench, or be occluded by the walls. Three factors determine whether a given point along the trench cross section will receive direct radiation or will be shaded: the sun's azimuth angle (ϕ) with respect to the trench orientation (ORI), the sun's elevation angle (φ), and the trench aspect ratio (depth/width).

To determine whether a point d is shaded or sunlit, the length of the shade normal to the trench orientation (L' in Fig. 2) is computed via:

$$L' = \frac{depth}{\tan(\varphi')} \tag{1}$$

where depth is the trench depth and φ' is the projected elevation angle on the normal to the trench orientation:

$$\tan(\varphi') = \frac{\tan(\varphi)}{\cos(\theta)} \tag{2}$$

and

$$\theta = |\phi - NOR| = |\phi - ORI + \pi/2| \tag{3}$$

NOR is the angle of the normal to the trench orientation, and ORI is the trench orientation relative to the north.

As illustrated in Fig. 3, when $ORI < \phi < (\pi + ORI)$ the point under consideration is shaded by wall 2 (case a). Thus, point d is shaded if $d > (width - L')$. When $(\pi + ORI) < \phi < (2\pi + ORI)$ the point is shaded by wall 1 (case b), and point d is shaded if $d < L'$ and sunlit otherwise.

2.2. Diffuse solar radiation

The radiation emanating from a point on the celestial hemisphere (dS) and reaching the point under consideration is (Berliner, 1989)

$$\Omega_O = \Omega \sin\beta dS \tag{4}$$

with dS defined as (Zhao et al., 2003)

$$dS = r^2 \sin\psi d\alpha d\psi \tag{5}$$

β and following scales are illustrated in Fig. 4.

Since

$$\begin{aligned} AQ &= r\sin\beta \\ AP &= r\sin\psi \\ AQ &= AP\sin\alpha = r\sin\psi\sin\alpha \end{aligned} \tag{6}$$

$$\sin\beta = \sin\psi\sin\alpha \tag{7}$$

And Eq. (4) is rewritten as

$$\Omega_O = \Omega \sin\psi \sin\alpha dS \tag{8}$$

Combining Eqs. (5) and (8) yields

$$\Omega_O = \Omega r^2 \sin^2\psi \sin\alpha d\alpha d\psi \tag{9}$$

The diffuse radiation reaching O emanating from a slice of the upper hemisphere with angle $\measuredangle BPA$ not occluded by the trench walls (the gray area in Fig. 4) is therefore

$$\Omega_S = \int_0^{2\pi} \int_{\varepsilon_1}^{\varepsilon_2} \Omega \sin^2\psi \sin\alpha d\psi d\alpha \tag{10}$$

where ε_1 and ε_2 are the meridional view angles (Fig. 5), and

$$\begin{aligned} \varepsilon_1 &= \arctan\frac{depth}{width - d} \\ \varepsilon_2 &= \pi - \sigma = \pi - \arctan\frac{depth}{d} \end{aligned} \tag{11}$$

Assuming the diffuse radiation is isotropic, the solution of Eq. (10) is

$$\Omega_S = \Omega r^2 [\cos\varepsilon_1 - \cos\varepsilon_2]\pi/2 \tag{12}$$

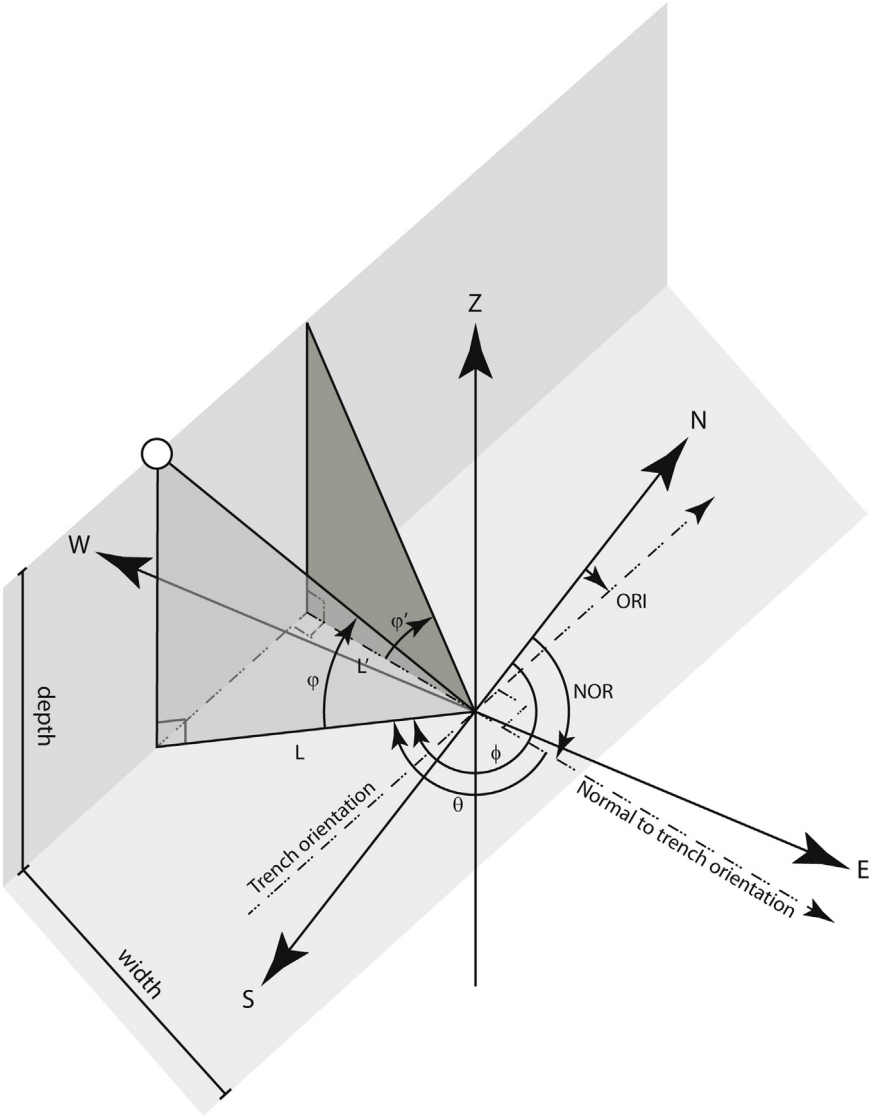

Fig. 2. Projection of direct solar radiation on the normal to the trench orientation.

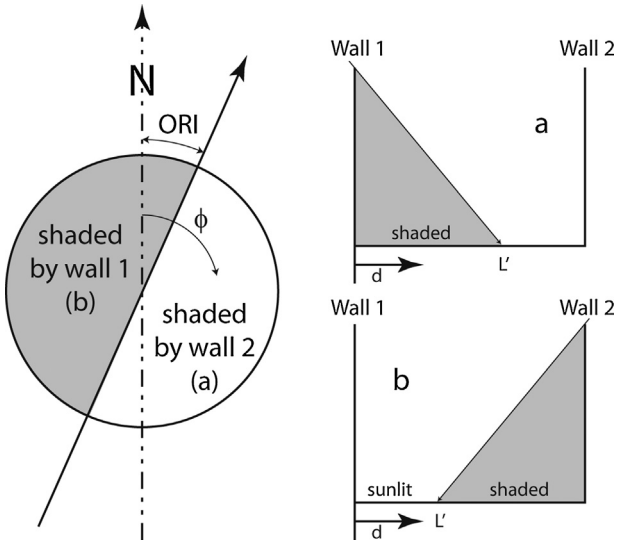

Fig. 3. Shaded and sunlit portions of the trench cross-section depending on the azimuth angle (ϕ); (a) when shade is formed by wall 1, and (b) when shade is formed by wall 2.

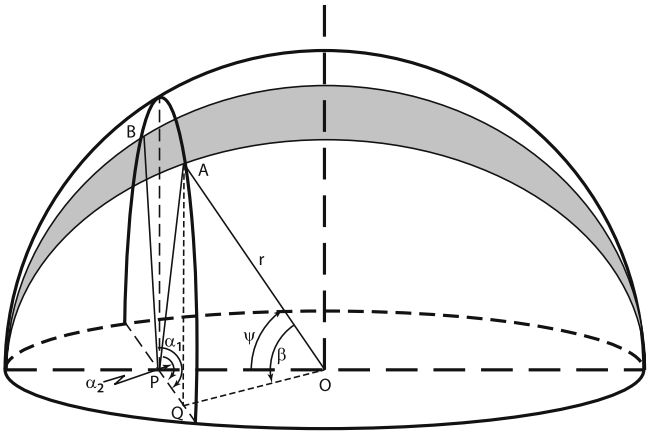

Fig. 4. Celestial hemisphere and elements required for the computation of diffuse radiation that emanates from a slice of the upper hemisphere (grayed) and reaches point O. $\beta \equiv \sphericalangle AOQ$; $\psi \equiv \sphericalangle APO$; $\alpha \equiv \sphericalangle APQ$.

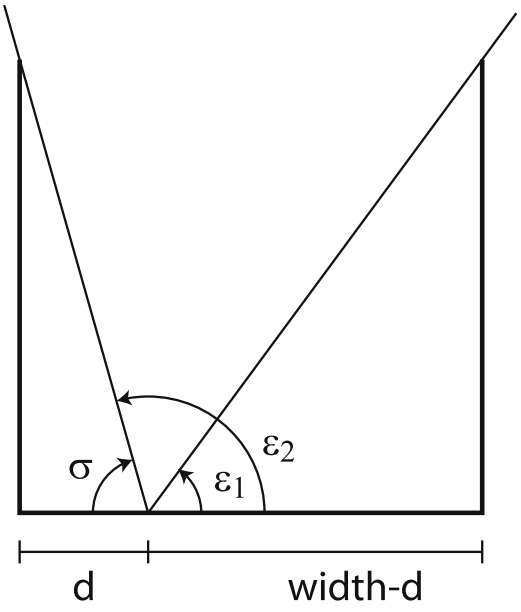

Fig. 5. View angles perpendicular to the trench floor at a distance d from the left wall.

Normalizing by the diffuse radiation from the entire celestial hemisphere (ΩU)

$$\frac{\Omega_S}{\Omega_U} = \frac{\Omega r^2 \left[\cos\varepsilon_1 - \cos\varepsilon_2\right]\pi/2}{\Omega r^2 \int_0^{\pi}\int_0^{\pi} \sin^2\psi \sin\alpha d\psi d\alpha} \tag{13}$$

yields the fraction of diffuse radiation reaching a given point on the trench floor (FracDiff):

$$FracDiff = \frac{\cos\varepsilon_1 - \cos\varepsilon_2}{2} \tag{14}$$

The diffuse radiation is the diffuse radiation reaching a point d on the trench floor is the product of the diffuse radiation on a horizontal plane outside the trench (DiffRAD) and FracDiff.

2.3. Radiation reflected from walls

Assuming the walls are Lambertian reflectors, the radiation reflected back from the wall (RefWall) depends on the total radiation reaching the wall (WRAD; direct + diffuse) and on the wall's albedo (ρ):

$$RefWall = \rho WRAD = REF_{DIR} + REF_{DIF} \tag{15}$$

REF_{DIR} and REF_{DIF} are the direct and diffuse radiation reflected from the wall, respectively.

2.3.1. Direct radiation reflected from walls

Based on Lambert's Cosine law, the beam intensity of the direct solar radiation (Beam, illustrated in Fig. 6) is

$$Beam = \frac{DIR}{\sin\varphi} \tag{16}$$

where DIR is the direct radiation measured on a horizontal surface.

The intensity of direct radiation reaching the trench wall (WDIR) is computed by

$$WDIR = Beam \sin\left(\pi/2 - \varphi\right) = Beam\cos\varphi \tag{17}$$

The depth to which the wall is illuminated (h_{REF}, Fig. 7) depends on the aspect ratio of the trench, the sun's elevation angle, and the sun's azimuth angle relative to the trench orientation of the wall, and is computed by

$$h_{REF} = width \tan\varphi' \tag{18}$$

The direct radiation reflected from a wall and reaching a point d on the trench floor is

$$REF_{DIR} = \rho \cdot WDIR \cdot FracRefDIR \tag{19}$$

In which FracRefDIR is the fraction of the illuminated wall as seen from point d, computed similarly to the diffused radiation following Eq. (14), in which ε_1 and ε_2 specified in Fig. 7, depend on the trench orientation and the sun's azimuth:

$$\begin{aligned} ORI < AZI < (\pi + ORI) \rightarrow \{ & \quad \varepsilon_1 = \operatorname{atan}\left(\frac{depth}{d}\right) \\ & \quad \varepsilon_2 = \operatorname{atan}\left(\frac{depth - h_{REF}}{d}\right) \\ (\pi + ORI) < AZI < (2\pi + ORI) \rightarrow \{ & \quad \varepsilon_1 = \operatorname{atan}\left(\frac{depth}{width - d}\right) \\ & \quad \varepsilon_1 = \operatorname{atan}\left(\frac{depth - h_{REF}}{width - d}\right) \end{aligned} \tag{20}$$

2.3.2. Diffuse radiation reflected from walls

The diffuse radiation reaching a given point on the wall (x_i) is limited by the fraction of the sky seen from this point (Fig. 8).

The fraction of diffuse radiation can be computed similarly to the fraction of diffuse radiation reaching a given point on the trench

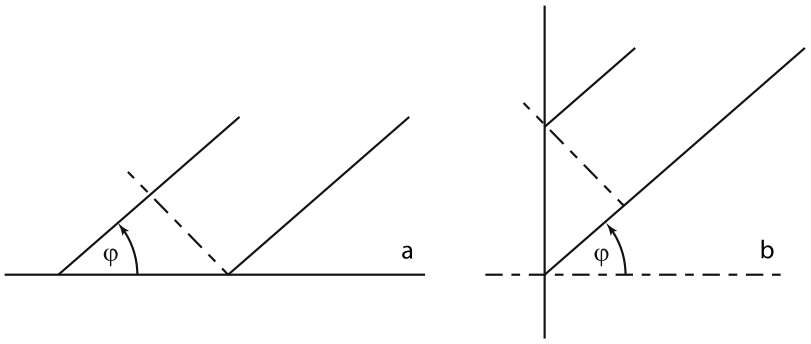

Fig. 6. The intensity of direct solar radiation projected on the trench wall. (a) The direct solar radiation beam projected on a horizontal surface; and (b) the same beam projected on a vertical surface (e.g., the trench wall).

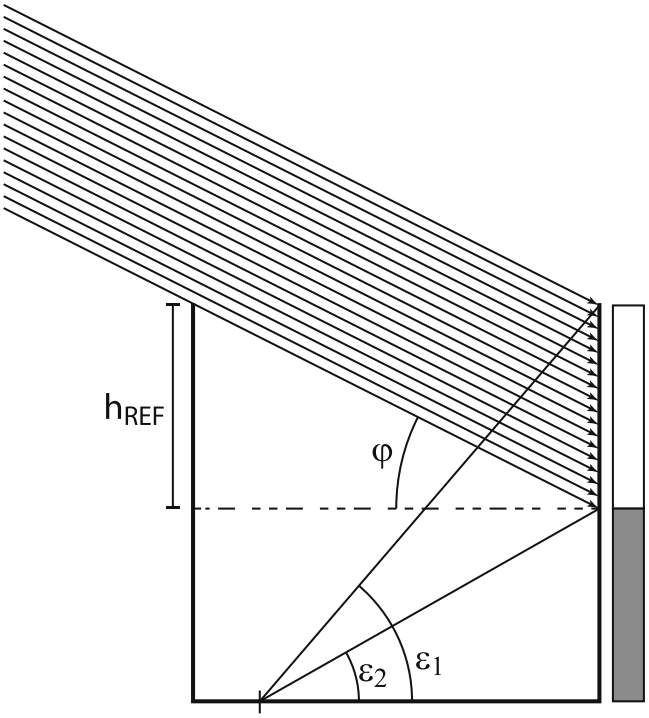

Fig. 7. The fraction of reflected radiation from the illuminated part of the wall seen by a specific point on the trench floor.

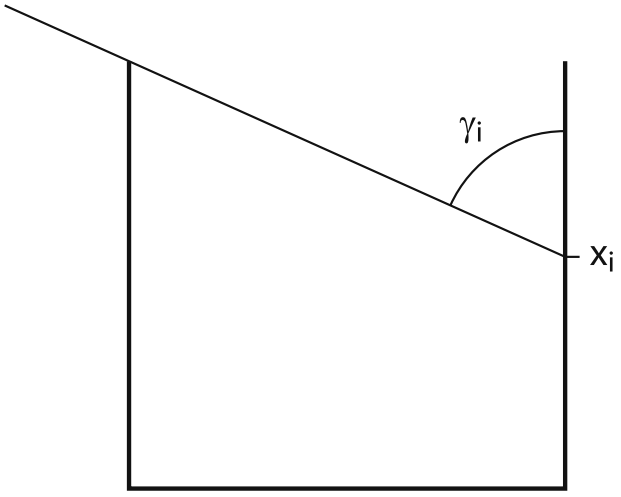

Fig. 8. The angle determining the fraction of the skies seen from point x on the wall.

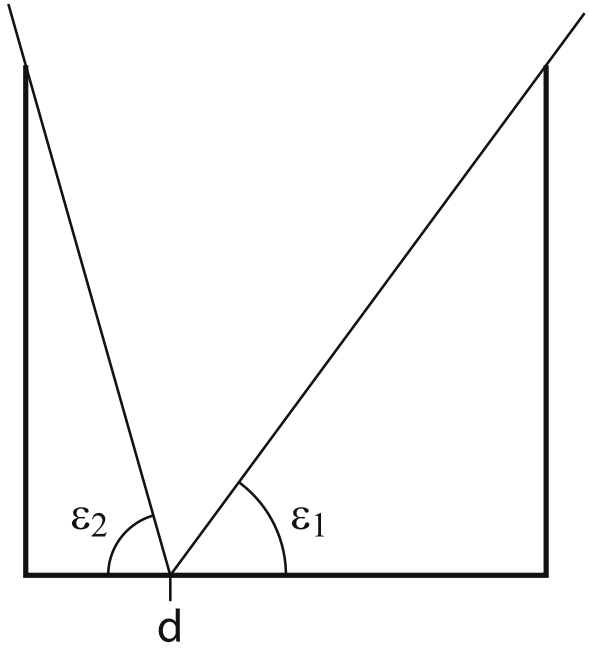

Fig. 9. The angles determining the amount of reflected radiation reaching point d on the trench floor.

floor, using Eq. (14), and since in this case ε_1 always equals 0, the fraction of diffused radiation in point x is

$$FracDiffWall = \frac{1 - \cos\gamma_i}{2} \tag{21}$$

γ_i is defined in Fig. 8. The diffuse radiation intensity at point x is then

$$WDIF_i = DiffRAD \cdot FracDiffWall_i \tag{22}$$

The diffuse radiation from each of the two walls is computed by dividing the wall into thin intervals and computing $WDIF_i$ for each interval, with

$$WDIF = \sum_{i=1}^{n} WDIF \tag{23}$$

n being the number of intervals.

The reflected diffuse radiation reaching point d on the bottom of the trench is then

$$FracRefDIF = \frac{1 - \cos\varepsilon_1}{2} + \frac{1 - \cos\varepsilon_2}{2} = 1 - \frac{\cos\varepsilon_1 + \cos\varepsilon_2}{2} \tag{24}$$

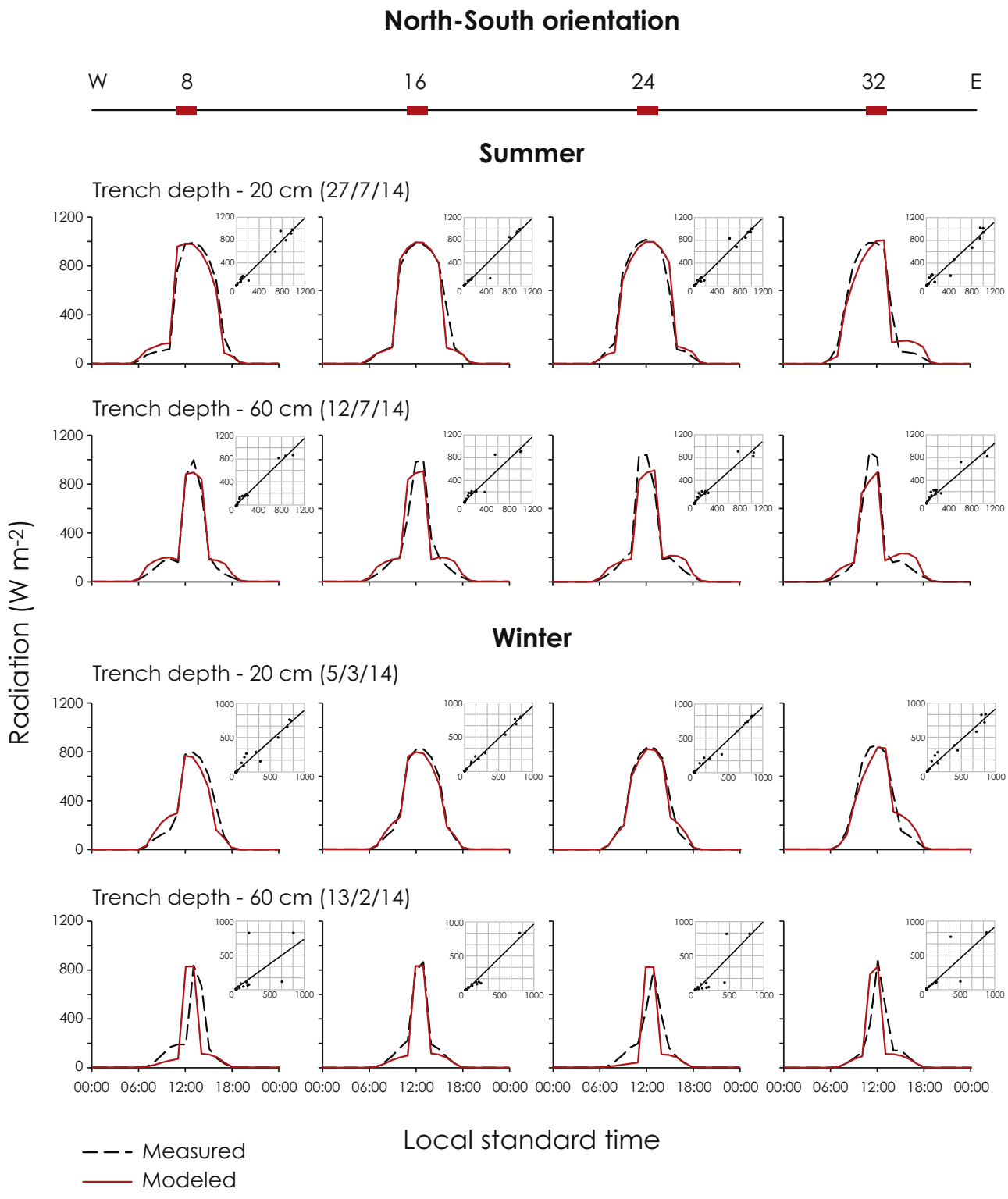

Fig. 10. Model validation: diurnal course of modeled and measured radiation inside a North-South trench with 40 cm width and depths of 20 and 60 cm at 4 positions across the trench – 8, 16, 24, and 32 cm from the western wall – for clear sky conditions in summer and winter.

in which ε_1 and ε_2 depicted in Fig. 9 are

$$\varepsilon_1 = \mathrm{a\,tan}\left(\frac{depth}{width - d}\right)$$
$$\varepsilon_2 = \mathrm{a\,tan}\left(\frac{depth}{d}\right) \quad (25)$$

The total amount of diffuse radiation reflected from the walls and reaching point d is therefore

$$REF_{DIF} = \rho \cdot WDIF \cdot FracRefDiff \quad (26)$$

Note that in quantifying the amount of radiation reaching the trench walls the radiation reflected from the opposite wall was

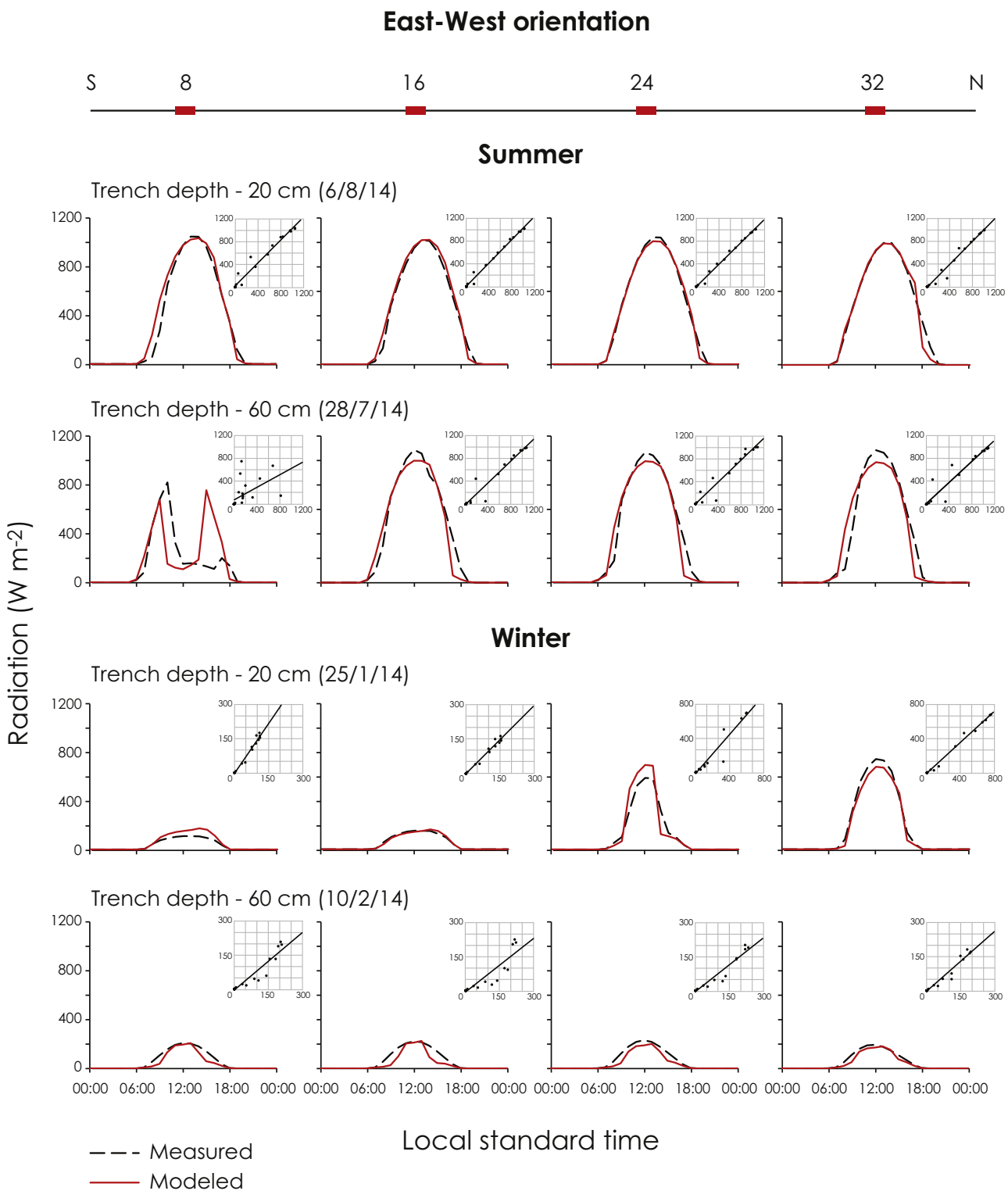

Fig. 11. Model validation: diurnal course of modeled and measured radiation inside an East-West trench with 40 cm width and depths of 20 and 60 cm at 4 positions across the trench – 8, 16, 24, and 32 cm from the southern wall – for clear sky conditions in summer and winter.

neglected. This may introduce a small error to the estimated radiation reaching the trench floor, which is assumed negligible under most conditions. This error will increase with albedo and with trench aspect ratio, both are unlikely to dominate in practice.

3. Model validation

The model was validated against measurements carried out throughout 2014 at the Jacob Bluestein Institutes for Desert

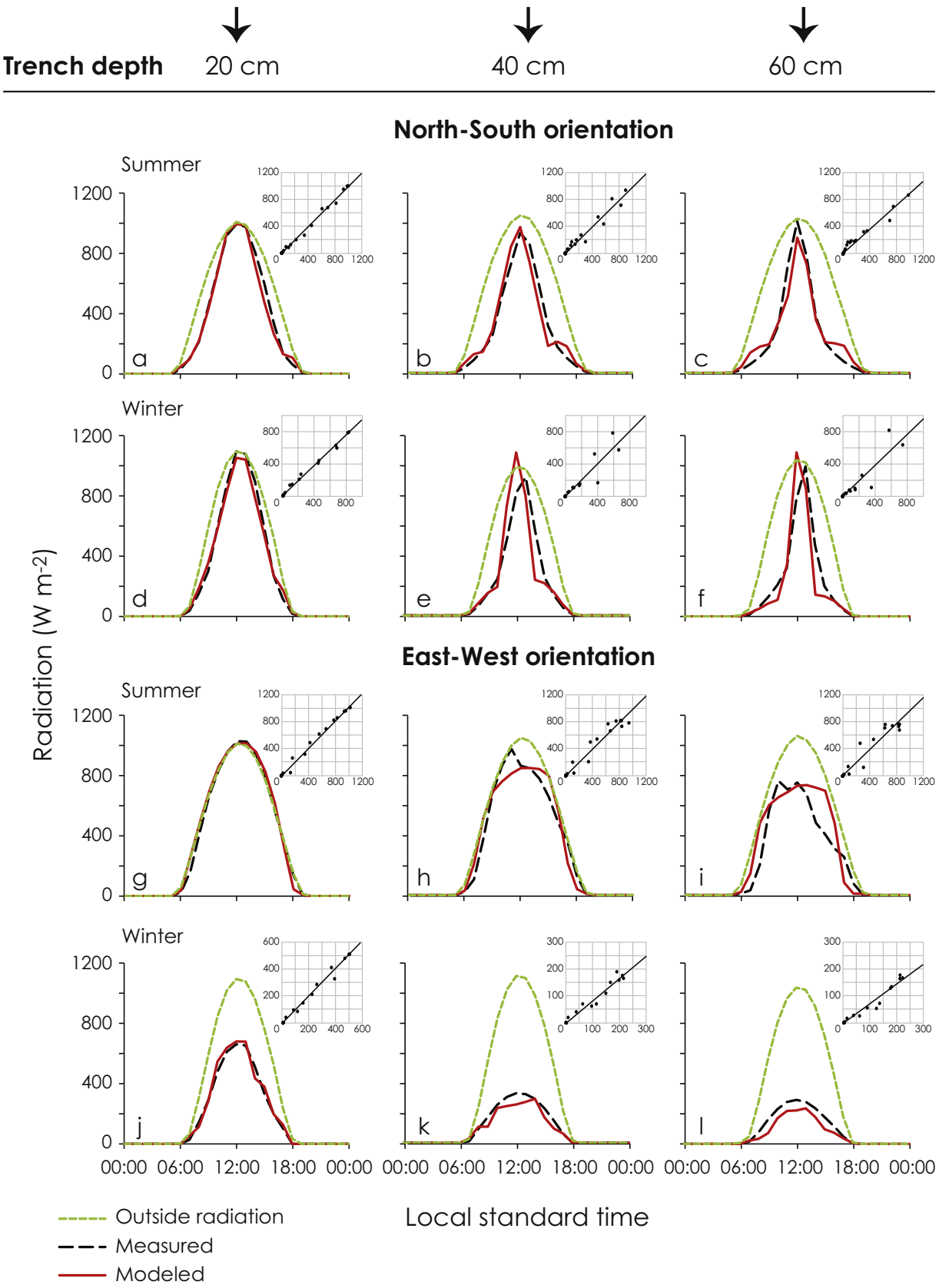

Fig. 12. Model validation: modeled and measured average radiation inside a 40-cm wide trench with depths of 20, 40, and 60 cm, oriented north-south and east-west along with solar radiation outside the trench. The scatter plot inserts are modeled (Y) vs. measured (X) for each diurnal course.

Table 1
Statistic results of model validation for the four locations where measurements were made inside a 0.4 m wide trench: 0.8, 0.16, 0.24, and 0.32 m, for the north-south (N-S) orientation distances are from the eastern wall, and for the east-west (E-W) orientation from the northern wall. Slope and r^2 are results of a linear regression between modeled results and measured data. Slopes not significantly different than one are italicized. All regressions were statistically significant. MAE is mean absolute error.

	Season	Depth	Loc1			Loc2			Loc3			Loc4		
			Slope [−]	r^2 [−]	MAE [MJ]	Slope [−]	r^2 [−]	MAE [MJ]	Slope [−]	r^2 [−]	MAE [MJ]	Slope [−]	r^2 [−]	MAE [MJ]
N-S	Summer	0.2 m	*0.99*	0.98	2.58	*1.00*	0.97	1.74	*0.99*	0.98	2.01	*0.93*	0.96	3.80
		0.6 m	*0.98*	0.98	2.13	*0.95*	0.92	3.38	0.89	0.96	3.09	0.86	0.95	3.52
	Winter	0.2 m	0.90	0.96	2.56	0.96	0.99	1.33	0.95	0.99	1.40	0.91	0.96	2.88
		0.6 m	*0.73*	0.45	5.49	*0.98*	0.98	1.57	*1.02*	0.77	4.08	*0.91*	0.72	3.36
E-W	Summer	0.2 m	*1.01*	0.97	2.79	*1.03*	0.99	1.86	*0.99*	1.00	1.23	*1.01*	0.98	1.89
		0.6 m	0.55	0.28	8.31	*0.96*	0.96	3.15	*0.96*	0.96	3.56	*0.93*	0.93	4.53
	Winter	0.2 m	1.47	0.98	1.30	*1.00*	0.98	0.36	1.15	0.94	2.71	0.92	0.99	1.74
		0.6 m	0.85	0.91	1.17	0.79	0.84	1.66	0.79	0.95	1.40	0.88	0.96	0.80

Table 2
Comparison of average modeled vs. measured radiation. Daily sum is the total amount of radiation that reached the trench floor ($\overline{R_{floor}}$). Daily fraction is $\overline{R_{floor}}$ divided by the total daily radiation outside the trench ($R_{outside}$). Slope and r^2 are results of a linear regression between modeled results and measured data. Slopes not significantly different than one are italicized. All regressions were statistically significant. MAE is mean absolute error.

	Season	Depth	Daily sum [MJ]		Daily fraction [−]		Linear regression		MAE	MAE/ Daily sum
			Observed	Modeled	Observed	Modeled	Slope	r^2	[MJ]	[%]
N-S	Summer	20 cm	546	538	0.78	0.77	*1.00*	0.99	1.31	0.24
		40 cm	399	422	0.55	0.59	*1.03*	0.99	1.58	0.40
		60 cm	335	352	0.48	0.50	0.93	0.99	1.74	0.52
	Winter	20 cm	390	380	0.80	0.78	0.95	1.00	0.99	0.25
		40 cm	233	235	0.57	0.57	*1.00*	0.87	2.85	1.23
		60 cm	215	195	0.47	0.43	*0.99*	0.86	2.72	1.26
E-W	Summer	20 cm	685	700	0.98	1.01	*1.01*	0.99	1.68	0.24
		40 cm	595	611	0.85	0.87	*1.00*	0.94	4.29	0.72
		60 cm	571	561	0.81	0.79	*0.95*	0.95	4.12	0.72
	Winter	20 cm	200	192	0.54	0.52	0.96	0.99	0.64	0.32
		40 cm	123	94	0.33	0.25	0.80	0.96	1.17	0.95
		60 cm	120	89	0.27	0.20	0.83	0.93	1.22	1.02

Table 3
Average and standard deviation (STD) of the monthly fraction of radiation reaching the trench floor from the outside radiation throughout the year.

		Aspect ratio				
		0.25	0.5	0.75	1	1.5
N-S	Average	0.84	0.71	0.60	0.51	0.39
	SDT	0.01	0.02	0.02	0.02	0.03
E-W	Average	0.85	0.71	0.58	0.50	0.40
	SDT	0.09	0.17	0.23	0.24	0.23

Research, Ben-Gurion University of the Negev, in the Negev highlands (31°08′N, 34°53′E, 400 m a.m.s.l.). The small mean annual precipitation (90 mm spanning between November and March) and large number of clear sky days made it possible to validate the model for a large range of sun azimuth and elevation angles.

3.1. Field measurements

A wooden trench (6 m long and 0.4 m wide) was built to depths of 0.2, 0.4, and 0.6 m corresponding to aspect ratios (depth/width) of 0.5, 1, and 1.5, respectively. The trench was alternately oriented north-south (N-S) or east-west (E-W). The albedo of the wood ($\rho = 0.56$) was determined using a portable Analytical Spectral Devices (ASD) FieldSpec spectrometer with a spectral range of 350–2500 nm and a spectral resolution of 1 nm.

Solar radiation was measured using 5 pyranometers (CMP3, Kipp & Zonen, Delft, The Netherlands). One pyranometer was positioned outside the trench and served as the reference incoming solar radiation, and four were positioned at the bottom of the trench at equal intervals (0.08, 0.16, 0.24, and 0.32 m from the northern/eastern wall). Pyranometer outputs were measured every 1 s and 15-min averages were recorded by a data-logger (CR21X, Campbell Scientific Ltd., Logan, UT, USA). Inter-calibration between the pyranometers was performed prior to the beginning (December 2013), and after the end (July 2014) of the measurement period. No change in the calibration coefficients was detected throughout the year.

For each of the 6 configurations (2 orientations × 3 depths) one day in winter and one day in summer with clear sky conditions were chosen and compared to model outputs. The model was configured to match the measurements with space intervals of 1 cm across the trench to allow selecting the exact locations of the pyranometers, which have a round black-body receptor with 1 cm diameter. Model outputs for each interval were saved. Model validation was performed both for individual locations and for the mean solar radiation reaching the trench floor ($\overline{R_{floor}}$). To match the average measured by the 4 pyranometers, modeled average radiation was computed using the four locations representing the locations of the pyranometers.

3.2. Validation results

Results for the north-south and east-west orientations are shown in Figs. 10 and 11, respectively, for depths 20 and 60 cm. Data for 40 cm showed similar results and are not presented. Overall, the model was capable of following the diurnal radiation course at each of the individual positions in both orientations and for both depths. Statistics of these relationships are presented in Table 1. The slopes of the regression lines were not significantly different from one for 60% of the cases. All regressions were statistically significant, with $r^2 > 0.90$ for 27 of the 32 cases and > 0.95 for 17 cases.

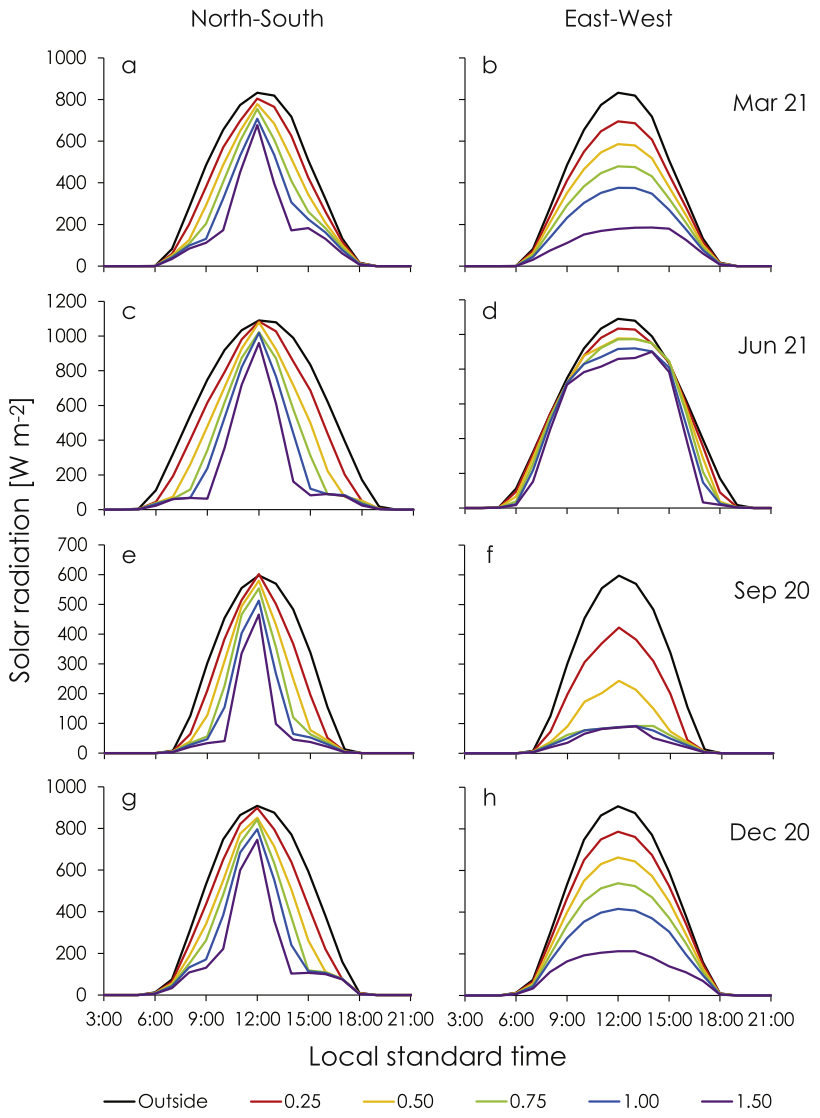

Fig. 13. Simulation results for a 1-m wide trench at depths of 0.25, 0.5, 0.75, 1.0, and 1.5 m oriented north-south and east-west at a representative day for each season.

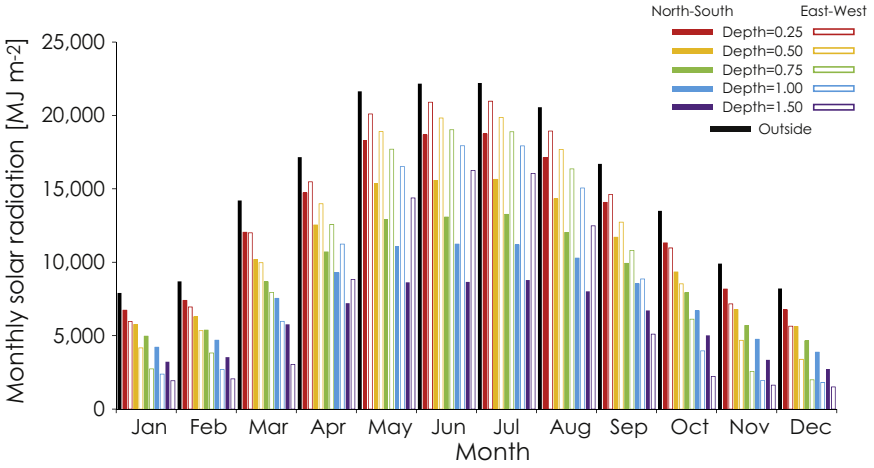

Fig. 14. Yearly course of monthly total incoming solar radiation outside and inside 1-m wide trenches with depth of 0.25, 0.5, 0.75, 1.0, 1.5 m oriented north-south and east-west.

In general, r^2 was somewhat lower for the 0.6 m depth compared to the 0.2 m depth in all locations and both orientations, indicating some minor inaccuracy in the models computation, possibly attributed to neglecting multiple reflections from the walls.

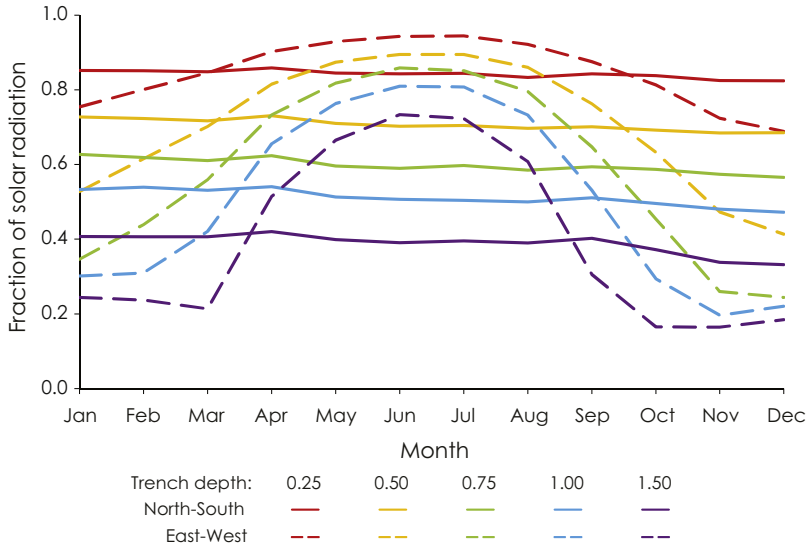

Fig. 15. Yearly course of monthly fraction of radiation inside and outside 1-m wide trenches with depth of 0.25, 0.5, 0.75, 1.0, 1.5 m oriented north-south and east-west.

Nevertheless, the mean absolute error (MAE; Hamilton, 1994), which was found to be the most appropriate measure of average error magnitude (Willmott and Matsuura, 2005) ranged from 0.36 to 8.31 MJ day^{-1}, corresponding to 0.17–2.81% of the total daily radiation reaching each point.

To examine the overall model performance, the modeled average radiation reaching the trench floor for all configurations was compared to the average measured data. The modeled averages were computed using the four locations corresponding to the measured positions. Comparison results are shown in Fig. 12 and Table 2. The modeled diurnal course follows quite closely the measured course with r^2 ranging from 0.86 to 1.00. The model performed slightly better in summer compared to winter and in shallower compared to deeper trenches. The E-W orientation in winter exhibited the greatest deviations, particularly at the 0.4 and 0.6 m depths, with a slope of 0.8 and 0.83, respectively. However, the MAE was lower than the summer cases, with a small relative error (MAE divided by daily sum of radiative flux in the trench ranging from 0.3 to 1%). This is due to the overall small amount of radiation reaching the trench in these two cases. Very good performance was found for the 0.2 m depth, or aspect ratio of 0.5, in both seasons and orientations with a slope of 0.95–1.0, $r^2 = 0.99$, and maximum MAE of 1.68 MJ. It is concluded that the model accurately depicts the diurnal course of radiation reaching the trench floor in both N-S and E-W orientations, in summer as well as in winter with a slight decrease in accuracy with increasing depth.

4. Model simulations and potential utility

Aiming to optimally design trench dimensions and orientation for minimizing solar radiation load within the trench (prime driver of soil evaporation), multiple model simulations were ran. Discrete model inputs included longitude-latitude coordinates (30.855375, 34.780739); time zone (GMT + 2); wall albedo (0.2); and the trench dimensions (constant width of 1 m, and depths of 0.25, 0.5, 0.75, 1, and 1.5 m) and orientations—north-south (N-S) and east-west (E-W). The trench was assumed infinitely long. The interval between model nodes across the trench width was 5 cm. Continuous data included hourly data of global and diffuse radiation measured by a meteorological station at the Jacob Bluestein Institutes for Desert Research, Ben-Gurion University of the Negev from January 1 01:00 to December 31 24:00 2006. $\overline{R_{floor}}$ was computed as the average of radiation reaching the 20 points across the interrow.

Distinct differences in the diurnal course of $\overline{R_{floor}}$ were observed between the N-S and E-W orientations (Fig. 13). While in both orientations $\overline{R_{floor}}$ decreased with depth, in the N-S orientation the diurnal curve was steeper with a sharp peak at noon, especially in the deeper configurations. This pattern repeated itself throughout the year, as exemplified by the plotted four days—the longest, shortest, autumn equinox, and spring equinox (or 1–2 days before/after with clear sky conditions). The daily course in the E-W orientation did not exhibit the peaks observed in the N-S orientation.

A large difference was observed between the four days for the E-W orientation—in the longest day there was little difference between the various depths, mostly from 09:00 to 15:00, while in the shortest day a very large difference between depths was observed throughout all light hours. Interestingly, the curves for the two equinox days were not similar, even though symmetry could have been expected. In the spring there is a more gradual decrease in $\overline{R_{floor}}$ with depth and an overall larger intensity compared to the autumn. This is likely due to the difference in the atmospheric optical thickness resulting in large difference in the incoming diffuse radiation flux for both days (mean fraction of diffuse radiation outside the trench between 09:00–15:00 was 0.4 and 0.2 for spring and autumn, respectively).

The effectiveness of the trenches as runoff agricultural systems will, to a large extent, be dependent on the degree of attenuation of total amount of radiation reaching the trench floor, at seasonal scales. The monthly total $\overline{R_{floor}}$ at the various depths for two orientations along with the fraction $\overline{R_{floor}}/R_{outside}$ are presented in Figs. 14 and 15, respectively. In the N-S orientation, $\overline{R_{floor}}/R_{outside}$ is practically constant throughout the year, and its magnitude determined only by the trench aspect ratio. A trench with aspect ratio of 0.25 will result in a steady reduction of ~15%, while a trench with aspect ratio of 1.5 will result with ~70% reduction (see Table 3 for the exact numbers for all configurations). In contrast to the N-S orientation, a clear yearly dependence in $\overline{R_{floor}}/R_{outside}$ is observed for the E-W orientation. In a trench with aspect ratio of 1.5 the reduction in the radiation flux was as high as ~85% in winter, and as low as ~25% in summer. For a trench with aspect ratio of 0.25 the corresponding values were ~30% and ~5%. Thus while the trench aspect ratio determines $\overline{R_{floor}}/R_{outside}$ for the N-S orientation, in the E-W orientation the season has a larger effect on $\overline{R_{floor}}/R_{outside}$. This finding has important implications for the design of trench runoff systems.

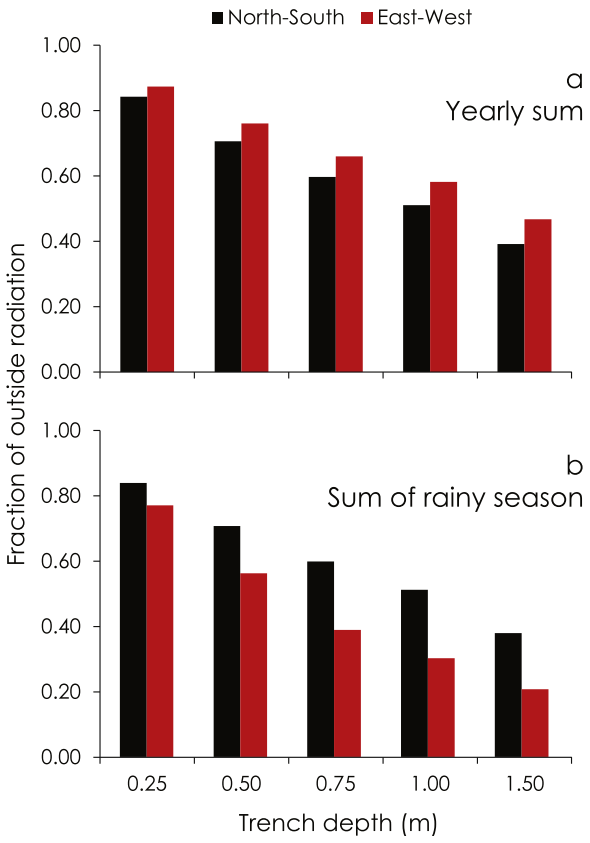

Fig. 16. Fraction of total radiation inside and outside 1-m wide trenches with depth of 0.25, 0.5, 0.75, 1.0, 1.5 m oriented north-south and east-west: (a) yearly sums; (b) sum over the rainy season.

Runoff systems are most efficient in regions where water is scarce and precipitation events are sporadic and intense. In many of these regions, the rainy season is short and the time interval between them long. The critical period for minimizing evaporative losses is therefore during the rainy season during which rain and hence runoff events occur. The orientation of the trench plays therefore a major role in determining the efficiency of the system. In this case study, the overall yearly $\overline{R_{floor}}/R_{outside}$ indicates higher radiation reaching a trench oriented E-W compared to a N-S oriented trench (Table 3 and Fig. 16a) at all depths, with an increasing difference with depth. If only the rainy months (November-March; Fig. 16b) are considered however, the trends are opposite. In this case the N-S oriented trenches receive more radiation than the E-W oriented trenches. In an area with typical Mediterranean climate as the Negev highlands, the best strategy would be to design trenches with E-W orientation. Determination of the actual depth and geometry of the trench depends on additional issues and will likely vary from place to place. The proposed model, will allow quantitatively assessment of the potential reduction in radiation load for any given configuration .

5. Conclusions

The model described herein computes the radiation reaching the floor of a trench at each point across the trench width accounting for the direct, diffuse, and reflected components. Model validation indicated that the model accurately depicts the diurnal course of radiation reaching the trench floor in both north-south and east-west orientations, in summer as well as in winter, with a slight decrease in accuracy with increasing depth.

Aiming to optimally design trench dimensions and orientation for minimizing solar radiation load within the trench in the Negev Desert, multiple model simulations were ran. Distinct differences in the diurnal course of mean solar radiation reaching the trench floor were observed between the north-south and east-west orientations. The yearly fraction of mean solar radiation reaching the trench floor to yearly total radiation outside the trench indicates that the radiation load in a trench oriented east-west is higher compared to a north-south oriented trench. Considering the rainy season only (November through March), this trend reverses, and radiation load is greater in the north-south orientation. Thus, aiming to reduce evaporative losses from trench-like runoff harvesting systems in the Negev, east-west orientated trenches are advantageous.

References

Berliner, P.R., 1989. Contribution of Heat Dissipated at the Soil Surface to the Energy Balance of a Citrus Orchard. PhD Thesis. The Hebrew University, Rehovot, 111 pp.
Boers, T.M., Benasher, J., 1982. A review of rainwater harvesting. Agric. Water Manage. 5 (2), 145–158.
Critchley, W., Siegert, K., 1991. Water Harvesting: A Manual for the Design and Construction of Water Harvesting Schemes for Plant Production. FAO, Rome.
Droppelmann, K., Berliner, P., 2003. Runoff agroforestry—a technique to secure the livelihood of pastoralists in the Middle East. J. Arid Environ. 54 (3), 571–577.
Erell, E., Williamson, T., 2006. Simulating air temperature in an urban street canyon in all weather conditions using measured data at a reference meteorological station. Int. J. Climatol. 26 (12), 1671–1694.
Evenari, M., Shanan, L., Tadmor, N., 1971. The Negev—The Challenge of a Desert. Harward University Press, Cambridge, Massachusettes, 345 pp.
Hamilton, J.D., 1994. Time Series Analysis. Princeton University Press.
Millennium Ecosystem Assessment, 2005. Ecosystems and Human Well-being: Synthesis. Island Press, Washington, DC.
Oke, T.R., 1981. Canyon geometry and the nocturnal urban heat island: comparison of scale model and field observations. J. Climatol. 1 (3), 237.
Oke, T.R., 1988. Street design and urban canopy layer climate. Energy Build. 11 (1–3), 103–113.
Terjung, W.H., Orourke, P.A., 1980a. Influences of physical structures on urban energy budgets. Boundary Layer Meteorol. 19 (4), 421–439.
Terjung, W.H., Orourke, P.A., 1980b. Simulating the casual elements of urban heat islands. Boundary Layer Meteorol. 19 (1), 93–118.
Willmott, C.J., Matsuura, K., 2005. Advantages of the mean absolute error (MAE) over the root mean square error (RMSE) in assessing average model performance. Clim. Res. 30, 79–82.
Zhang, S., Carmi, G., Berliner, P., 2013. Efficiency of rainwater harvesting of microcatchments and the role of their design. J. Arid Environ. 95, 22–29.
Zhao, W.G., Qualls, R.J., Berliner, P.R., 2003. Modeling of the short wave radiation distribution in an agroforestry system. Agric. Forest Meteorol. 118 (3–4), 185–206.